PERGAMON

International Journal of Solids and Structures 39 (2002) 4501–4524

INTERNATIONAL JOURNAL OF SOLIDS and STRUCTURES

www.elsevier.com/locate/ijsolstr

A piezoelectric material strip with a crack perpendicular to its boundary surfaces

B.L. Wang [a,c,*], Y.-W. Mai [b,c]

[a] Center for Composite Materials, Harbin Institute of Technology, Harbin 150001, PR China
[b] Department of Mechanical and Mechatronic Engineering, Centre for Advanced Materials Technology (CAMT), The University of Sydney, Sydney NSW 2006, Australia
[c] Department of Manufacturing Engineering and Engineering Management (MEEM), City University of Hong Kong, Tat Chee Avenue, Kowloon Tong, Hong Kong

Received 19 July 2001; received in revised form 9 May 2002

Abstract

A cracked piezoelectric material strip under combining mechanical and electrical loads is considered. The crack is vertical to the top and bottom edges of the strip. The edges of the strip are parallel to the x-axis and perpendicular to the z-axis. When a piezoelectric ceramic is poled, it exhibits transversely isotropic behavior. Among many possible poled axis orientations, a particular orientation when the poling direction lies parallel to x-axis is examined in this paper. Both impermeable crack and permeable crack assumptions are considered. Numerical results are included for three kinds of fracture mechanics specimens, namely an edge-cracked strip, a double edge-cracked strip, and a center-cracked strip, subjected to uniform tensions and uniform electric displacement loads simultaneously, at the far ends. In addition, an edge-cracked strip under pure bending and uniform electric displacement loads at the far ends is also investigated in this paper.

Keywords: Fracture; Electromechanical; Piezoelectric; Crack

1. Introduction

Piezoelectric materials have been extensively applied over the last decades to diverse areas such as electromechanical transducers, electronic packaging, solar projector, thermal sensors, underwater acoustic, and medical ultrasonic imaging. A significant disadvantage of piezoelectric materials, such as piezoelectric ceramics, is their brittleness. Stress concentrations at the defects produced during the manufacturing and/or service process, such as cavities, cracks, dislocations, inclusions and debondings, can contribute to critical crack growth and subsequent mechanical failure or dielectric breakdown. The understanding of the fracture

* Corresponding author.
E-mail address: wangbl2001@hotmail.com (B.L. Wang).

0020-7683/02/$ - see front matter
PII: S0020-7683(02)00378-5

process of piezoelectric materials could provide information to improve the design of electromechanical devices.

One of the most important and basic issues of studying fracture mechanics of piezoelectric materials is the electric boundary condition on the crack surface. Here, a crack is defined as a notch or an elliptic cavity without thickness and the crack interior is filled with air (not be filled with conductive medium). Taking into account the permittivity of the medium filling the crack, increases the complexity of the problem significantly (Hao and Shen, 1994; Balke et al., 1997). Therefore, it is commonly used to employ the idealized boundary conditions on the crack faces. One commonly used boundary condition is the specification that the normal component of electric displacement on the crack faces equals zero (Pak, 1990). This boundary condition ignores the electric field within the crack, based on the fact that the permittivity of piezoceramics is three orders of magnitude higher than the one of air or vacuum (Suo et al., 1992; Park and Sun, 1995a,b). The other commonly used boundary condition treats the crack as being electrically permeable (Mikahailov and Parton, 1990; Shindo et al., 2000; Kwon and Lee, 2000). Sosa (1991) has investigated the mechanical and electric fields in the vicinity of circular and elliptically holes and used the asymptotic expressions for the electromechanical fields in the vicinity of a crack to study the electric fields effects on crack arrest and crack skewing. Pak and Tobin (1993) found the ratio of the crack tip electric field to the applied field approaches unity as an elliptical cavity reduces to a slit. Dunn (1994) also investigated the effects of crack face boundary conditions on the energy release rate in piezoelectric solids. An elliptical cylinder cavity in a piezoelectric material was considered by Zhang and Tong (1996) to investigate the boundary conditions on the cavity surface. In the limiting process, they found that the two commonly used boundary conditions are actually the two extremes of the exact boundary conditions. Zhang et al. (1998) formulated the analytical solutions for an elliptical cylinder cavity or a crack inside infinite piezoelectric medium under combined mechanical–electrical loadings via the Stroh formalism and well confirmed by finite element analysis. Both conducting and insulating crack are considered to study the energy release rate for the crack propagation. In a recent paper, fracture of a finite height piezoelectric medium under combining electrical and mechanical loads was considered for two kinds of commonly used crack face boundary conditions (Wang et al., 2000a,b). The result showed that according to permeable crack model, the electric loads would have no influence on the singular stress and electric displacement ahead of the crack tip. Consequently, if this model is used to analyze the crack instability, the applied electric displacement load would contribute nothing to the fracture load. Such a conclusion would contradict experimental findings for it finds that the presence of an electric load can either promote or retard crack growth, depending on the magnitude and the direction of the electric load. On the other hand, based on the impermeable crack assumption, the failure strength for a piezoelectric material under combined electric mechanical load has been qualitatively predicated (Fulton and Gao, 2001; Sih and Zuo, 2000; Soh et al., 2001; Wang, 2000; Wang and Noda, 2000, 2001a). It is found that solutions based on impermeable crack assumption could be applied with a reasonable degree of confidence to the fracture prediction of the piezoelectric materials. In fact, recent work has showed that the impermeable crack assumption is a good one to the fracture of piezoelectric materials, and the permeable assumption is still not able to predict the fracture strength of piezoelectric materials correctly (Fulton and Gao, 2001).

With the increasingly wide application of smart materials and structures, the structure of a piezoelectric ceramic attached to a different material is of great importance. Hence, it is necessary to investigate the interfacial crack problem in structural components containing piezoelectric materials. The problem of cracks in laminated piezoelectric media has also received much attention. For example, Suo et al. (1992) analyzed the generalized two-dimensional problem of collinear interfacial cracks between dissimilar piezoelectric media, and gave the structure of singular fields near the crack tips. Beom and Atluri (1996) addressed the interfacial crack problem in piezoelectric materials. Their work is also based on the impermeable crack assumption. Recently, Qin and Mai (1999) investigated the thermal problem of interfacial cracks in piezoelectric solids. A plane strain problem for an interface crack is investigated by Herrmann

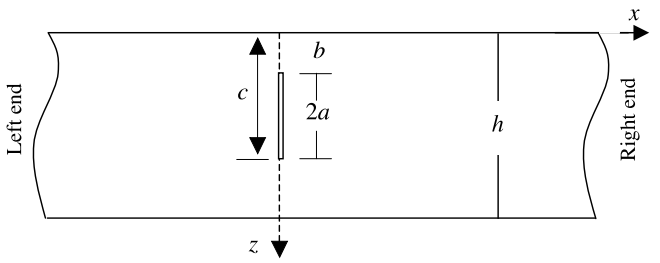

Fig. 1. A piezoelectric material strip poled along x-axis, the crack length $2a = c - b$. If b is larger than zero the crack is embedded in the strip. For an edge crack problem, b equals zero.

et al. (2001). The contact zone model with an artificial zone is considered for electrically impermeable crack. The fracture mechanics responses of multi-layered piezoelectric media were considered for anti-plane cracks (Wang et al., 1998, 2000b) and axisymmetric cracks (Wang and Noda, 2001b).

This paper investigates the fracture mechanics problem of a piezoelectric material strip under in plane electromechanical loading. The crack orientates in a direction normal to the surfaces of the strip, as shown in Fig. 1. Both embedded crack and edge crack are considered. Fourier transforms technique is used to reduce the problem to the solution of singular integral equations. Two kinds of commonly used crack surface boundary conditions are considered. Numerical results are shown graphically to illustrate the effects of crack size and crack position on the stress and electric displacement intensity factors for different crack face boundary condition assumptions.

2. The solution of the piezoelectric elasticity

We consider a two-dimensional plane strain problem, the medium is transversely isotropic and x is the poling direction, then the constitutive equations can be written as

$$\begin{Bmatrix} \sigma_{zz} \\ \sigma_{xx} \\ \tau_{xz} \\ D_z \\ D_x \end{Bmatrix} = \begin{bmatrix} c_{11} & c_{13} & 0 & 0 & -e_{31} \\ c_{13} & c_{33} & 0 & 0 & -e_{33} \\ 0 & 0 & c_{44} & -e_{15} & 0 \\ 0 & 0 & e_{15} & \epsilon_{11} & 0 \\ e_{31} & e_{33} & 0 & 0 & \epsilon_{33} \end{bmatrix} \begin{Bmatrix} \partial w/\partial z \\ \partial u/\partial x \\ \partial w/\partial x + \partial u/\partial z \\ E_z \\ E_x \end{Bmatrix}, \tag{1}$$

where u and w are, respectively, the x and z components of the displacement vector; c_{11}, c_{13}, c_{33}, and c_{44} are elastic constants; e_{31}, e_{33} and e_{15} are piezoelectric constants; ϵ_{11} and ϵ_{33} stand for dielectric permittivities; τ_{xz}, σ_{zz} and σ_{xx} are stress components; D_x and D_z are electric displacements. The electric field components E_x and E_y may be written in terms of electric potential ϕ as

$$E_x = -\phi_{,x}, \quad E_z = -\phi_{,z}. \tag{2}$$

The plane piezoelasticity problem requires the solution of the following equilibrium equations:

$$\left.\begin{aligned} &c_{11}\frac{\partial^2 w}{\partial z^2} + c_{44}\frac{\partial^2 w}{\partial x^2} + (c_{13}+c_{44})\frac{\partial^2 u}{\partial x \partial z} + (e_{31}+e_{15})\frac{\partial^2 \phi}{\partial x \partial z} = 0 \\ &(c_{13}+c_{44})\frac{\partial^2 w}{\partial x \partial z} + c_{44}\frac{\partial^2 u}{\partial z^2} + c_{33}\frac{\partial^2 u}{\partial x^2} + e_{15}\frac{\partial^2 \phi}{\partial z^2} + e_{33}\frac{\partial^2 \phi}{\partial x^2} = 0 \\ &(e_{31}+e_{15})\frac{\partial^2 w}{\partial x \partial z} + e_{15}\frac{\partial^2 u}{\partial z^2} + e_{33}\frac{\partial^2 u}{\partial x^2} - \epsilon_{11}\frac{\partial^2 \phi}{\partial z^2} - \epsilon_{33}\frac{\partial^2 \phi}{\partial x^2} = 0 \end{aligned}\right\}, \tag{3}$$

where u, w are the x, z components of the displacement vector.

The geometries of the strip and the crack are shown in Fig. 1. The applied loads are considered to be symmetric with respect to $x = 0$ plane such that

$$\tau_{xz}(0,z) = 0, \tag{4}$$

$$u(0,z) = 0, \quad \phi(0,z) = 0, \quad z \notin [b,c]. \tag{5}$$

The crack problem can be treated by means of the superposition technique. That is one first solved the problem without crack and then use the equal and opposite value of the stresses and electric displacement on the cracked plane as the applied loads on the crack faces. Suppose the crack is mechanically free of surface traction. Denote D_0 as the normal component of the electric displacement on the crack faces (D_0 is zero for impermeable crack and unknown for permeable crack). Then, the boundary conditions on the cracked plane $x = 0$ can be stated as follows:

$$\sigma_{xx}(0,z) = -\sigma_{\infty}(z), \quad z \in [b,c], \tag{6}$$

$$D_x(0,z) = D_0(z) - D_{\infty}(z), \quad z \in [b,c], \tag{7}$$

where $\sigma_{\infty}(z)$ and $D_{\infty}(z)$ are the values obtained from the solution without crack. They can be resulted from mechanical, electrical and/or thermal loads.

On the top surface $z = 0$, the traction and electric charge free boundary conditions are

$$\tau_{xz}(x,0) = 0, \quad \sigma_{zz}(x,0) = 0, \quad D_z(x,0) = 0. \tag{8}$$

On the bottom surface $z = h$, two kinds of boundary conditions are considered, the first one is the traction and electric charge free boundary conditions

$$\tau_{xz}(x,h) = 0, \quad \sigma_{zz}(x,h) = 0, \quad D_z(x,h) = 0, \tag{9a}$$

and the second one is that the strip stretches freely but without bending

$$\tau_{xz}(x,h) = 0, \quad \partial w(x,h)/\partial x = 0, \quad D_z(x,h) = 0. \tag{9b}$$

Due to the symmetry with respect to $x = 0$ plane, it is sufficient to consider only the right part of the medium ($x > 0$). The general solution of the governing equations (3) for displacements and electric potential can be expressed in terms of unknown coefficients $G_n(\xi)$ in the following forms:

$$u_g = \frac{1}{2\pi}\int_{-\infty}^{\infty} B_{1n} G_n e^{|\xi|\lambda_n x} e^{-i\xi z}\, d\xi, \tag{10a}$$

$$v_g = \frac{1}{2\pi}\int_{-\infty}^{\infty} B_{2n} G_n e^{|\xi|\lambda_n x} e^{-i\xi z}\, d\xi, \tag{10b}$$

$$\phi_g = \frac{1}{2\pi}\int_{-\infty}^{\infty} B_{3n} G_n e^{|\xi|\lambda_n x} e^{-i\xi z}\, d\xi. \tag{10c}$$

By substituting Eqs. (10a)–(10c) into Eq. (3), we have

$$\begin{bmatrix} c_{44} - c_{33}\lambda_n^2 & i\,\mathrm{sgn}(\xi)(c_{13} + c_{44})\lambda_n & e_{15} - e_{33}\lambda_n^2 \\ i\,\mathrm{sgn}(\xi)(c_{13} + c_{44})\lambda_n & c_{11} - c_{44}\lambda_n^2 & i\,\mathrm{sgn}(\xi)(e_{31} + e_{15})\lambda_n \\ e_{15} - e_{33}\lambda_n^2 & i\,\mathrm{sgn}(\xi)(e_{31} + e_{15})\lambda_n & -\epsilon_{11} + \epsilon_{33}\lambda_n^2 \end{bmatrix} \begin{Bmatrix} B_{1n} \\ B_{2n} \\ B_{3n} \end{Bmatrix} = 0, \tag{11}$$

where $i = \sqrt{-1}$, $\mathrm{sgn}(\xi)$ equals 1 for positive values of ξ, and 1 for negative values of ξ. Equation (11) is an eigenvalue problem. Nontrivial eigenvector B_{jn} ($j = 1, 2, 3$) exist if λ_n is a root of the determinant, i.e.,

$$\begin{vmatrix} c_{44}-c_{33}\lambda_n^2 & \mathrm{i}\,\mathrm{sgn}(\xi)(c_{13}+c_{44})\lambda_n & e_{15}-e_{33}\lambda_n^2 \\ \mathrm{i}\,\mathrm{sgn}(\xi)(c_{13}+c_{44})\lambda_n & c_{11}-c_{44}\lambda_n^2 & \mathrm{i}\,\mathrm{sgn}(\xi)(e_{31}+e_{15})\lambda_n \\ e_{15}-e_{33}\lambda_n^2 & \mathrm{i}\,\mathrm{sgn}(\xi)(e_{31}+e_{15})\lambda_n & -\epsilon_{11}+\epsilon_{33}\lambda_n^2 \end{vmatrix} = 0. \tag{12}$$

Since the stresses and electric displacements vanish as x approaches infinity, the eigenvalues for λ_n are selected such that

$$\mathrm{Re}(\lambda_n) < 0. \tag{13}$$

Therefore, there are three roots for λ_n.

Because the medium is finite, the part solution of the governing equations (3) should be included to consider the boundary conditions on the surface of the medium. We express the partial solution of (3) in terms of unknown coefficients $F_m(s)$ in the following form:

$$u_p = \frac{2}{\pi}\int_0^\infty A_{1m}\sin sx F_m \mathrm{e}^{s\lambda_m z}\,\mathrm{d}s, \tag{14a}$$

$$w_p = \frac{2}{\pi}\int_0^\infty A_{2m}\cos sx F_m \mathrm{e}^{s\lambda_m z}\,\mathrm{d}s, \tag{14b}$$

$$\phi_p = \frac{2}{\pi}\int_0^\infty A_{3m}\sin sx F_m \mathrm{e}^{s\lambda_m z}\,\mathrm{d}s. \tag{14c}$$

By substituting Eqs. (14a)–(14c) into Eq. (3), we can get the following characteristic equations to determine eigenvalues λ_m and the corresponding eigenvectors (A_{1m}, A_{2m}, A_{3m})

$$\begin{bmatrix} c_{44}\lambda_m^2-c_{33} & -(c_{13}+c_{44})\lambda_m & e_{15}\lambda_m^2-e_{33} \\ -(c_{13}+c_{44})\lambda_m & c_{44}-c_{11}\lambda_m^2 & -(e_{31}+e_{15})\lambda_m \\ e_{15}\lambda_m^2-e_{33} & -(e_{31}+e_{15})\lambda_m & \epsilon_{33}-\epsilon_{11}\lambda_m^2 \end{bmatrix} \begin{Bmatrix} A_{1m} \\ A_{2m} \\ A_{3m} \end{Bmatrix} = 0, \tag{15}$$

It is clear that there are six roots for λ_m.

The complete solutions for Eq. (3) are the sum of the general solution and the partial solution:

$$u(x,z) = \frac{2}{\pi}\int_0^\infty \sin sx \sum_{m=1}^{6} A_{1m}\mathrm{e}^{s\lambda_m z}F_m\,\mathrm{d}s + \sum_{n=1}^{3}\frac{1}{2\pi}\int_{-\infty}^{\infty}\mathrm{e}^{|\xi|\lambda_n x}B_{1n}\mathrm{e}^{-\mathrm{i}\xi z}G_n\,\mathrm{d}\xi, \tag{16a}$$

$$w(x,z) = \frac{2}{\pi}\int_0^\infty \cos sx \sum_{m=1}^{6} A_{2m}\mathrm{e}^{s\lambda_m z}F_m\,\mathrm{d}s + \sum_{n=1}^{3}\frac{1}{2\pi}\int_{-\infty}^{\infty}\mathrm{e}^{|\xi|\lambda_n x}B_{2n}\mathrm{e}^{-\mathrm{i}\xi z}G_n\,\mathrm{d}\xi, \tag{16b}$$

$$\phi(x,z) = \frac{2}{\pi}\int_0^\infty \sin sx \sum_{m=1}^{6} A_{3m}\mathrm{e}^{s\lambda_m z}F_m\,\mathrm{d}s + \sum_{n=1}^{3}\frac{1}{2\pi}\int_{-\infty}^{\infty}\mathrm{e}^{|\xi|\lambda_n x}B_{3n}\mathrm{e}^{-\mathrm{i}\xi z}G_n\,\mathrm{d}\xi, \tag{16c}$$

where F_m and G_n $(m = 1,\ldots,6, n = 1,2,3)$ are unknown functions of variables s and ξ, respectively. The corresponding stresses and electric displacements are given by

$$\tau_{xz}(x,z) = \frac{2}{\pi}\sum_{m=1}^{6}\int_0^\infty s\sin sx C_{1m}\mathrm{e}^{s\lambda_m z}F_m\,\mathrm{d}s + \sum_{n=1}^{3}\frac{1}{2\pi}\int_{-\infty}^{\infty}\xi\mathrm{e}^{|\xi|\lambda_n x}D_{1n}\mathrm{e}^{-\mathrm{i}\xi z}G_n\,\mathrm{d}\xi, \tag{17}$$

$$\sigma_{zz}(x,z) = \frac{2}{\pi}\sum_{m=1}^{6}\int_0^\infty s\cos sx C_{2m}\mathrm{e}^{s\lambda_m z}F_m\,\mathrm{d}s + \sum_{n=1}^{3}\frac{1}{2\pi}\int_{-\infty}^{\infty}\xi\mathrm{e}^{|\xi|\lambda_n x}D_{2n}\mathrm{e}^{-\mathrm{i}\xi z}G_n\,\mathrm{d}\xi, \tag{18}$$

$$D_z(x,z) = \frac{2}{\pi}\sum_{m=1}^{6}\int_0^\infty s\sin sxC_{3m}e^{s\lambda_m z}F_m\,ds + \sum_{n=1}^{3}\frac{1}{2\pi}\int_{-\infty}^{\infty}\xi e^{|\xi|\lambda_n x}D_{3n}e^{-i\xi z}G_n\,d\xi, \tag{19}$$

$$\sigma_{xx}(x,z) = \frac{2}{\pi}\sum_{m=1}^{6}\int_0^\infty s\cos sxC_{4m}e^{s\lambda_m z}F_m\,ds + \sum_{n=1}^{3}\frac{1}{2\pi}\int_{-\infty}^{\infty}\xi e^{|\xi|\lambda_n x}D_{4n}e^{-i\xi z}G_n\,d\xi, \tag{20}$$

$$D_x(x,z) = \frac{2}{\pi}\sum_{m=1}^{6}\int_0^\infty s\cos sxC_{5m}e^{s\lambda_m z}F_m\,ds + \sum_{n=1}^{3}\frac{1}{2\pi}\int_{-\infty}^{\infty}\xi e^{|\xi|\lambda_n x}D_{5n}e^{-i\xi z}G_n\,d\xi, \tag{21}$$

where the coefficients $C_{jm}s$ and $D_{jn}(\xi)$ $(j = 1,\ldots,5)$ are given in Appendix A.

3. The singular integral equations

To make the solution satisfy the mixed mode boundary conditions (4)–(8), (9a), (9b) we introduce the following auxiliary functions $g_u(z)$ and $g_\phi(z)$ on the cracked plane:

$$g_u(z) = \partial u(0,z)/\partial z, \quad g_\phi(z) = \partial\phi(0,z)/\partial z. \tag{22}$$

From boundary condition (5), it follows that

$$g_u(z) = 0, \quad g_\phi(z) = 0, \quad z \notin [b,c]. \tag{23}$$

In the case of embedded crack problem ($b > 0$), $g_u(z)$ and $g_\phi(z)$ should satisfy the following single-valueness conditions:

$$\int_b^c g_u(z)\,dz = 0, \quad \int_b^c g_\phi(z)\,dz = 0. \tag{24}$$

In the case of edge crack problem ($b = 0$), the single-valueness conditions are no longer satisfied.

After substituting Eqs. (16a) and (16c) into Eq. (22), and by inverting the corresponding Fourier integrals we find

$$\sum_{n=1}^{3}B_{1n}G_n = i\xi^{-1}\int_b^c g_u(r)e^{i\xi r}\,dr, \tag{25}$$

$$\sum_{n=1}^{3}B_{3n}G_n = i\xi^{-1}\int_b^c g_\phi(r)e^{i\xi r}\,dr. \tag{26}$$

Condition (4) requires that

$$\sum_{n=1}^{3}D_{1n}G_n = 0. \tag{27}$$

It follows from Eqs. (25)–(27) that

$$G_n(\xi) = i\xi^{-1}\int_b^c [b_{nu}(\xi)g_u(r) + b_{n\phi}(\xi)g_\phi(r)]e^{i\xi r}\,dr, \quad n = 1,2,3, \tag{28}$$

where the coefficients b_{nu} and $b_{n\phi}$ $(n = 1, 2, 3)$ are given in Appendix B.

By applying Eqs. (17)–(19) and (28) to homogeneous boundary conditions (8), (9a) and (9b), and by inverting the corresponding Fourier sine and cosine integrals, we obtain

$$[G]\{F\} = \frac{1}{2s}\int_b^c \left[\{f_u(s,r)\}g_u(r) + \{f_\phi(s,r)\}g_\phi(r)\right] \mathrm{d}r \tag{29}$$

where $\{F\} = \{F_m\}$, the vectors $\{f_u\}$ and $\{f_\phi\}$, and the matrix $[G]$ are given in Appendix C.

The linear algebraic equations (29) can be used to determine all of the remaining unknowns F_m $(m = 1, \ldots, 6)$, in terms of g_u and g_ϕ, the results are

$$F_m = \frac{1}{2s}\int_b^c \left[\chi_{mu}(s,r)g_u(r) + \chi_{m\phi}(s,r)g_\phi(r)\right] \mathrm{d}r, \quad m = 1, \ldots, 6, \tag{30}$$

where the coefficients $\chi_{mu}(s,r)$ and $\chi_{m\phi}(s,r)$ $(m = 1, \ldots, 6)$, are

$$\{\chi_u\} = [G]^{-1}\{f_u\}, \quad \{\chi_\phi\} = [G]^{-1}\{f_\phi\}. \tag{31}$$

By substituting Eqs. (28) and (30) into Eqs. (20) and (21) one get the stress σ_{xx} and the electric displacement D_x. At the cracked plane $(x = 0)$, we have

$$\int_b^c [\Lambda(z,r)]\begin{Bmatrix} g_u(r) \\ g_\phi(r) \end{Bmatrix}\mathrm{d}r + \int_b^c [H(z,r)]\begin{Bmatrix} g_u(r) \\ g_\phi(r) \end{Bmatrix}\mathrm{d}r = \begin{Bmatrix} \sigma_{xx}(0,z) \\ D_x(0,z) \end{Bmatrix}, \tag{32}$$

where the kernels $[\Lambda]$ and $[H]$ are given by

$$[\Lambda(z,r)] = -\frac{1}{2\pi \mathrm{i}}\int_{-\infty}^{\infty}\sum_{n=1}^{3}\begin{bmatrix} D_{4n}b_{nu} & D_{4n}b_{n\phi} \\ D_{5n}b_{nu} & D_{5n}b_{n\phi} \end{bmatrix} \mathrm{e}^{\mathrm{i}\xi(r-z)}\,\mathrm{d}\xi, \tag{33}$$

$$[H(z,r)] = \frac{1}{\pi}\int_0^{\infty}\sum_{m=1}^{6}\begin{bmatrix} C_{4m}\chi_{mu}(s,r) & C_{4m}\chi_{m\phi}(s,r) \\ C_{5m}\chi_{mu}(s,r) & C_{5m}\chi_{m\phi}(s,r) \end{bmatrix} \mathrm{e}^{s\lambda_m z}\,\mathrm{d}s. \tag{34}$$

It can be easily shown from Appendixes A and B that

$$-\sum_{n=1}^{3}\begin{bmatrix} D_{4n}b_{nu} & D_{4n}b_{n\phi} \\ D_{5n}b_{nu} & D_{5n}b_{n\phi} \end{bmatrix} = \mathrm{sgn}(\xi)[\Lambda_0], \tag{35}$$

where $[\Lambda_0]$ is a constant matrix which depends only on the material properties. It follows from Eqs. (33) and (35) that

$$[\Lambda(z,r)] = \frac{1}{\pi}[\Lambda_0]\frac{1}{r-z}. \tag{36}$$

The as-yet-unknown functions g_u and g_ϕ are determined by applying Eq. (32) to crack surface boundary conditions (6) and (7), the results are

$$\frac{1}{\pi}[\Lambda_0]\int_b^c \frac{1}{r-z}\begin{Bmatrix} g_u(r) \\ g_\phi(r) \end{Bmatrix}\mathrm{d}r + \int_b^c [H(z,r)]\begin{Bmatrix} g_u(r) \\ g_\phi(r) \end{Bmatrix}\mathrm{d}r = \begin{Bmatrix} -\sigma_\infty(z) \\ D_0(z) - D_\infty(z) \end{Bmatrix}, \quad z \in [b,c]. \tag{37}$$

In order to simplify the analysis, the integral interval $[b, c]$ is normalized by defining

$$(z,r) = \frac{c-b}{2}(\bar{z},\bar{r}) + \frac{c+b}{2}. \tag{38}$$

The integral Eq. (37) would then becomes

$$\frac{1}{\pi}[\Lambda_0]\int_{-1}^{1} \frac{1}{\bar{r}-\bar{z}}\begin{Bmatrix} g_u(r) \\ g_\phi(r) \end{Bmatrix}\mathrm{d}\bar{r} + a\int_{-1}^{1}[H(z,r)]\begin{Bmatrix} g_u(r) \\ g_\phi(r) \end{Bmatrix}\mathrm{d}\bar{r} = \begin{Bmatrix} -\sigma_\infty(z) \\ D_0(z) - D_\infty(z) \end{Bmatrix}, \quad \bar{z} \in [-1,1]. \tag{39}$$

This integral equations will be used to solve the auxiliary functions g_u and g_ϕ.

4. Stress and electric displacement intensity factors

Eq. (39) can be solved by applying the proper boundary conditions on the crack faces. As mentioned above, two kinds of electrical boundary conditions on the crack surface are usually considered. One commonly used boundary condition is that the crack is assumed to be impermeable to electric fields, i.e. the crack face is charge free and thus the electric displacement $D_0(z)$ vanishes everywhere inside the crack. According to this boundary condition, Eq. (39) becomes

$$\frac{1}{\pi}[\Lambda_0]\int_{-1}^{1}\frac{1}{\bar{r}-\bar{z}}\begin{Bmatrix} g_u(r) \\ g_\phi(r)\end{Bmatrix}\mathrm{d}\bar{r}+a\int_{-1}^{1}[H(z,r)]\begin{Bmatrix} g_u(r) \\ g_\phi(r)\end{Bmatrix}\mathrm{d}\bar{r}=-\begin{Bmatrix}\sigma_\infty(z) \\ D_\infty(z)\end{Bmatrix},\quad \bar{z}\in[-1,1]. \tag{40a}$$

The other commonly used boundary condition treats the crack as being electrically permeable, i.e., no electric potential jump across the crack. Therefore, $g_\phi=0$ and the normal component $D_0(z)$ of the electric displacement inside of the crack is unknown. It follows from Eq. (39) that the values of displacement jumps and $D_0(z)$ can be solved from the following equation:

$$\frac{1}{\pi}[\Lambda_0]\int_{-1}^{1}\frac{1}{\bar{r}-\bar{z}}\begin{Bmatrix} g_u(r) \\ 0\end{Bmatrix}\mathrm{d}\bar{r}+a\int_{-1}^{1}[H(z,r)]\begin{Bmatrix} g_u(r) \\ 0\end{Bmatrix}\mathrm{d}\bar{r}=\begin{Bmatrix}-\sigma_\infty(z) \\ D_0(z)-D_\infty(z)\end{Bmatrix},\quad \bar{z}\in[-1,1]. \tag{40b}$$

Eq. (40b) shows that for a permeable crack the displacement jump across the crack depends only on material properties and the applied mechanical loads, but not on the electrical displacement loads. Consequently, the stress and electric displacement intensity factors ahead of the crack tip are independent of applied electrical displacement load.

Integral equations (40a) and (40b) contain Cauchy-type kernels. In the case of edge crack problem, their solutions may be expressed as (Erdogan and Wu, 1996, 1997)

$$\begin{Bmatrix} g_u(r) \\ g_\phi(r)\end{Bmatrix}=\frac{1}{\sqrt{1-\bar{r}}}\sum_{n=0}^{\infty}\begin{Bmatrix} a_{nu} \\ a_{n\phi}\end{Bmatrix}T_n(\bar{r}), \tag{41}$$

where T_n is the Chebyshev polynomial of the first kind, a_{nu} and $a_{n\phi}$ are unknown coefficients. Applying Eq. (41) to Eqs. (40a) and (40b) and following the procedure outlined by Erdogan and Wu (1996, 1997), the following are obtained for the impermeable crack and the permeable crack, respectively:

$$\begin{aligned}&[\Lambda_0]\frac{1}{\pi}\frac{\log|B(\bar{z})|}{\sqrt{1-\bar{z}}}\sum_{n=0}^{\infty}\begin{Bmatrix} a_{nu} \\ a_{n\phi}\end{Bmatrix}T_n(\bar{z})+[\Lambda_0]\frac{1}{\pi}\sum_{n=0}^{\infty}\begin{Bmatrix} a_{nu} \\ a_{n\phi}\end{Bmatrix}\int_{-1}^{1}\frac{T_n(\bar{r})-T_n(\bar{z})}{\sqrt{1-\bar{r}}(\bar{r}-\bar{z})}\mathrm{d}\bar{r}\\&\quad+\frac{c}{2}\sum_{n=0}^{\infty}\left(\int_{-1}^{1}[H(z,r)]\frac{T_n(\bar{r})}{\sqrt{1-\bar{r}}}\mathrm{d}\bar{r}\right)\begin{Bmatrix} a_{nu} \\ a_{n\phi}\end{Bmatrix}=-\begin{Bmatrix}\sigma_\infty(z) \\ D_\infty(z)\end{Bmatrix},\end{aligned} \tag{42a}$$

and

$$\begin{aligned}&[\Lambda_0]\frac{1}{\pi}\frac{\log|B(\bar{z})|}{\sqrt{1-\bar{z}}}\sum_{n=0}^{\infty}\begin{Bmatrix} a_{nu} \\ 0\end{Bmatrix}T_n(\bar{z})+[\Lambda_0]\frac{1}{\pi}\sum_{n=0}^{\infty}\begin{Bmatrix} a_{nu} \\ 0\end{Bmatrix}\int_{-1}^{1}\frac{T_n(\bar{r})-T_n(\bar{z})}{\sqrt{1-\bar{r}}(\bar{r}-\bar{z})}\mathrm{d}\bar{r}\\&\quad+\frac{c}{2}\sum_{n=0}^{\infty}\left(\int_{-1}^{1}[H(z,r)]\frac{T_n(\bar{r})}{\sqrt{1-\bar{r}}}\mathrm{d}\bar{r}\right)\begin{Bmatrix} a_{nu} \\ 0\end{Bmatrix}=\begin{Bmatrix}-\sigma_\infty(z) \\ D_0(z)-D_\infty(z)\end{Bmatrix},\end{aligned} \tag{42b}$$

where

$$B(\bar{z})=\frac{1+\sqrt{(1-\bar{z})/2}}{1-\sqrt{(1-\bar{z})/2}}. \tag{43}$$

The linear equations (42a) and (42b) can be solved by truncating the series and using a collocation technique outlined by Erdogan and Wu (1996). Because of the symmetry of the problem, only mode I stress intensity factor K_{I} and electric displacement intensity factor K_{IV} exist, their values ahead of the crack tip ($z = c$) are defined and obtained as

$$\left\{ \begin{array}{c} K_{\mathrm{I}}(c) \\ K_{\mathrm{IV}}(c) \end{array} \right\} = \left(\sqrt{2(z-c)} \right)_{z \to c+0} \left\{ \begin{array}{c} \sigma_{xx}(z) \\ D_x(z) \end{array} \right\} = -\sqrt{c}[\Lambda_0] \sum_{n=0}^{\infty} \left\{ \begin{array}{c} a_{nu} \\ a_{n\phi} \end{array} \right\}. \tag{44}$$

The shape of the deformed crack $u(+0,z)$ and the electric potential on the crack face $\phi(+0,z)$ can be calculated from Eqs. (22) and (41)

$$\left\{ \begin{array}{c} u(+0,\bar{z}) \\ \phi(+0,\bar{z}) \end{array} \right\} = \sum_{n=0}^{\infty} \left\{ \begin{array}{c} a_{nu} \\ a_{n\phi} \end{array} \right\} \int_c^z \frac{1}{\sqrt{1-\bar{r}}} T_n(\bar{r})\, \mathrm{d}r. \tag{45}$$

It is found that

$$\left\{ \begin{array}{c} u(+0,\bar{z}) \\ \phi(+0,\bar{z}) \end{array} \right\} = -\frac{\sqrt{2}}{4} c \sum_{n=0}^{\infty} \left(\frac{\sin[(n-0.5)\alpha]}{n-0.5} + \frac{\sin[(n+0.5)\alpha]}{n+0.5} \right) \left\{ \begin{array}{c} a_{nu} \\ a_{n\phi} \end{array} \right\}, \tag{46}$$

where

$$\cos\alpha = (2z-c)/c. \tag{47}$$

Similarly, for the embedded crack problem the solution of Eqs. (40a) and (40b) has the following form:

$$\left\{ \begin{array}{c} g_u(r) \\ g_\phi(r) \end{array} \right\} = \frac{1}{\sqrt{1-\bar{r}^2}} \sum_{n=1}^{\infty} \left\{ \begin{array}{c} a_{nu} \\ a_{n\phi} \end{array} \right\} T_n(\bar{r}). \tag{48}$$

The application of Eq. (48) to Eqs. (40a) and (40b) yields:

$$[\Lambda_0] \sum_{n=1}^{\infty} \left\{ \begin{array}{c} a_{nu} \\ a_{n\phi} \end{array} \right\} U_{n-1}(\bar{z}) + a \sum_{n=1}^{\infty} \left(\int_{-1}^{1} [H(z,r)] \frac{T_n(\bar{r})}{\sqrt{1-\bar{r}^2}}\, \mathrm{d}\bar{r} \right) \left\{ \begin{array}{c} a_{nu} \\ a_{n\phi} \end{array} \right\} = -\left\{ \begin{array}{c} \sigma_\infty(z) \\ D_\infty(z) \end{array} \right\}, \tag{49a}$$

and

$$[\Lambda_0] \sum_{n=1}^{\infty} \left\{ \begin{array}{c} a_{nu} \\ 0 \end{array} \right\} U_{n-1}(\bar{z}) + a \sum_{n=1}^{\infty} \left(\int_{-1}^{1} [H(z,r)] \frac{T_n(\bar{r})}{\sqrt{1-\bar{r}^2}}\, \mathrm{d}\bar{r} \right) \left\{ \begin{array}{c} a_{nu} \\ 0 \end{array} \right\} = \left\{ \begin{array}{c} -\sigma_\infty(z) \\ D_0(z) - D_\infty(z) \end{array} \right\}, \tag{49b}$$

for the impermeable crack problem and the permeable crack problem, respectively, where U_n is the Chebyshev polynomial of the second kind. Again, the linear equations (49a) and (49b) are solved by truncating the series and using a collocation technique outlined by Erdogan and Wu (1996, 1997). In this paper, 10 terms ($n = 0, \ldots, 10$) are found to be sufficient to yield convergent results. After determining the coefficients a_{nu} and $a_{n\phi}$, the stress intensity factor K_{I} and the electric displacement intensity factor K_{IV} ahead of the crack tips at $z = b$ and $z = c$ can be defined and calculated as

$$\left\{ \begin{array}{c} K_{\mathrm{I}}(b) \\ K_{\mathrm{IV}}(b) \end{array} \right\} = \left(\sqrt{2(b-z)} \right)_{z \to b-0} \left\{ \begin{array}{c} \sigma_{xx}(z) \\ D_x(z) \end{array} \right\} = \sqrt{a}[\Lambda_0] \sum_{n=1}^{\infty} (-1)^n \left\{ \begin{array}{c} a_{nu} \\ a_{n\phi} \end{array} \right\}, \tag{50}$$

$$\left\{ \begin{array}{c} K_{\mathrm{I}}(c) \\ K_{\mathrm{IV}}(c) \end{array} \right\} = \left(\sqrt{2(z-c)} \right)_{z \to c+0} \left\{ \begin{array}{c} \sigma_{xx}(z) \\ D_x(z) \end{array} \right\} = -\sqrt{a}[\Lambda_0] \sum_{n=1}^{\infty} \left\{ \begin{array}{c} a_{nu} \\ a_{n\phi} \end{array} \right\}. \tag{51}$$

The shape of the deformed crack $u(+0,z)$ and the electric potential on the crack face $\phi(+0,z)$ for the embedded crack problem can be calculated from Eqs. (22) and (48)

$$\begin{Bmatrix} u(+0,\bar{z}) \\ \phi(+0,\bar{z}) \end{Bmatrix} = \sum_{n=1}^{\infty} \begin{Bmatrix} a_{nu} \\ a_{n\phi} \end{Bmatrix} \int_c^z \frac{1}{\sqrt{1-\bar{r}^2}} T_n(\bar{r})\,\mathrm{d}r. \tag{52}$$

It is found that

$$\begin{Bmatrix} u(+0,\bar{z}) \\ \phi(+0,\bar{z}) \end{Bmatrix} = -a \sum_{n=1}^{\infty} \frac{\sin n\alpha}{n} \begin{Bmatrix} a_{nu} \\ a_{n\phi} \end{Bmatrix}, \tag{53}$$

where

$$\cos\alpha = \frac{1}{a}\left(z - \frac{c+b}{2}\right). \tag{54}$$

The energy release rate G can be calculated by the crack closure integral technique, the result is

$$G = \frac{\pi}{2}\{K_{\mathrm{I}}, K_{\mathrm{IV}}\}[\Lambda_0]^{-1}\{K_{\mathrm{I}}, K_{\mathrm{IV}}\}^{\mathrm{T}}. \tag{55}$$

5. Numerical examples and discussions

In what follows, we pay our attentions to a PZT-5H piezoelectric ceramic strip. The values of the material constants are given by $c_{11} = 12.6 \times 10^{10}$ N/m^2, $c_{13} = 8.41 \times 10^{10}$ N/m^2, $c_{33} = 11.7 \times 10^{10}$ N/m^2, $c_{44} = 2.3 \times 10^{10}$ N/m^2, $e_{31} = -6.5$ C/m^2, $e_{33} = 23.3$ C/m^2, $e_{15} = 17.44$ C/m^2, $\epsilon_{11} = 150.3 \times 10^{-10}$ C/V m, $\epsilon_{33} = 130.0 \times 10^{-10}$ C/V m. Four kinds of crack geometries and loading conditions are considered:

(1) A strip contains an edge crack under a uniform tension and a uniform electric displacement at the far ends, as shown in Fig. 2.
(2) A strip contains an edge crack under a pure bending and a uniform electric displacement at the far ends, as shown in Fig. 3.
(3) A strip contains a double edge-crack under a uniform tension and a uniform electric displacement at the far ends, as shown in Fig. 4a. Due to the symmetry with respect to the mid-plane of the strip, it suffices to consider only half of the strip. The problem in Fig. 4a is equivalent to the problem in Fig. 4b.
(4) A center-cracked strip under a uniform tension and a uniform electric displacement at the far ends, as shown in Fig. 5.

In the following numerical analysis, we consider the region of applied electric displacement loads $D_\infty/(e_{33}/c_{33})\sigma_\infty = 0$, 1, 2, and 3. Those values are used based on the consideration that both negative electrical fields and positive electric fields are included in the analysis. The electric displacement load can be readily achieved in the laboratory by applying a constant potential difference across the specimen. The

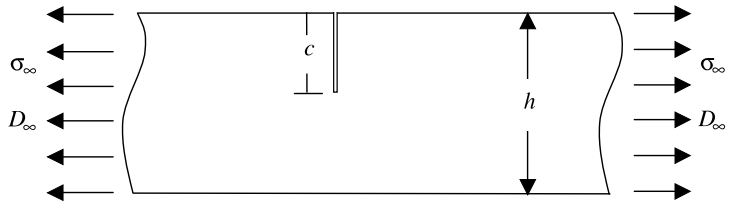

Fig. 2. A SEC piezoelectric material strip poled along x-axis. The strip undergoes a uniform tensile stress $\sigma_{xx} = \sigma_\infty$ and a uniform electric displacement $D_x = D_\infty$ at $x = \pm\infty$.

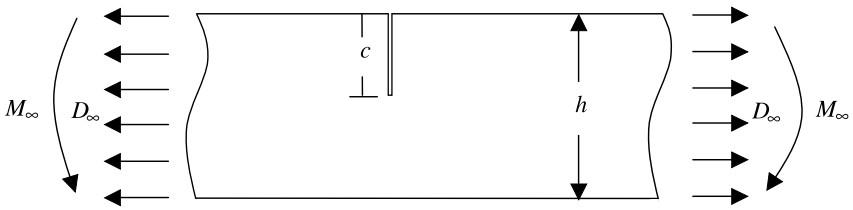

Fig. 3. A single edge cracked pure bending (SEB) piezoelectric material strip. The medium is poled along x-axis and undergoes a pure bend of moment M_∞ and a uniform electric displacement $D_x = D_\infty$ at $x = \pm\infty$.

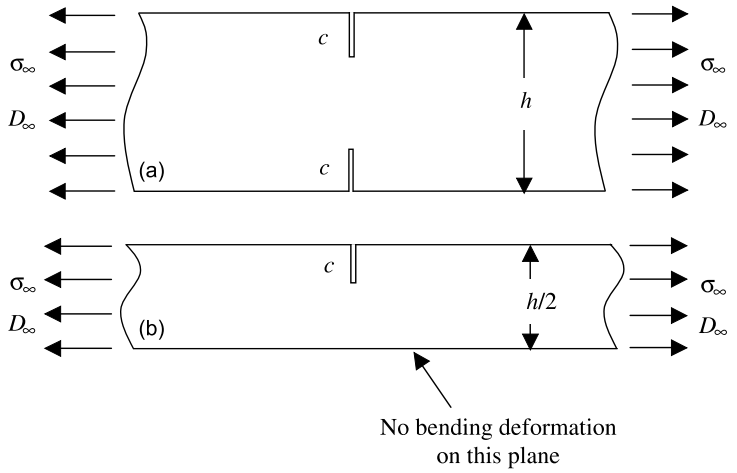

Fig. 4. (a) A DEC piezoelectric material strip poled along x-axis. The strip undergoes a uniform tensile stress $\sigma_{xx} = \sigma_\infty$ and a uniform electric displacement $D_x = D_\infty$ at $x = \pm\infty$. Due to the symmetry with respect to the mid-plane of the strip, only half of the strip is needed to be considered, the problem (a) is equivalent to the problem (b).

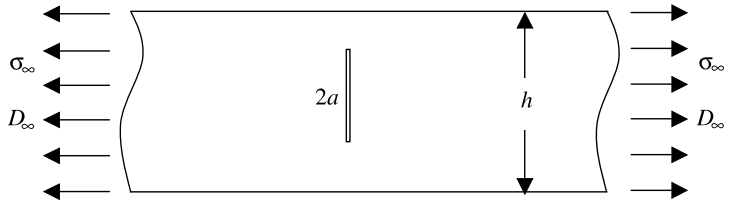

Fig. 5. A central crack in a piezoelectric material strip poled along x-axis. The strip undergoes a uniform tensile stress $\sigma_{xx} = \sigma_\infty$ and a uniform electric displacement $D_x = D_\infty$ at $x = \pm\infty$.

relationship between the electric displacement load and electric field load at the far ends can be found from the constitutive equation (1),

$$\sigma_{zz} = 0 = c_{11}\frac{\partial w}{\partial z} + c_{13}\frac{\partial u}{\partial x} - e_{31}E_\infty,$$

$$\sigma_\infty = c_{13}\frac{\partial w}{\partial z} + c_{33}\frac{\partial u}{\partial x} - e_{33}E_\infty,$$

$$D_\infty = e_{31}\frac{\partial w}{\partial z} + e_{33}\frac{\partial u}{\partial x} + \epsilon_{33}E_\infty.$$

Therefore,

$$D_\infty = \frac{c_{11}e_{33} - c_{13}e_{31}}{c_{11}c_{33} - c_{13}^2}\sigma_\infty + \left[\epsilon_{33} + \frac{c_{33}e_{31}^2 - 2c_{13}e_{31}e_{33} + c_{11}e_{33}^2}{c_{11}c_{33} - c_{13}^2}\right]E_\infty$$

for the PZT-5H piezoelectric ceramic considered, the result is

$$D_\infty = (4.541\sigma_\infty + 258.9E_\infty) \times 10^{-10} \quad (\mathrm{C/m^2}).$$

The corresponding electric field loads E_∞ for $D_\infty/(e_{33}/c_{33})\sigma_\infty = 0$, 1, 2, and 3 are $-0.01574\sigma_\infty$ (V/m), $-0.009848\sigma_\infty$ (V/m), $-0.002156\sigma_\infty$ (V/m), and $0.005536\sigma_\infty$ (V/m), respectively. Hence, both negative electric fields and positive electric field are included in the analysis.

Figs. 6–10 plot the stress intensity factors, the electric displacements intensity factors, the energy release rates, the deformed crack shapes, and the electric potentials on the crack face, respectively, for an edge-cracked strip under a uniform tension and a uniform electric displacement at the far ends. It is found that the stress intensity factor depends little on the applied electric displacement load D_0. The effects of the crack face electrical boundary condition assumptions on stress intensity factors are also found to be not significant. As a result there is only one curve in Fig. 6 for any values of D_0.

Fig. 7 depicted the dependence of the electric displacement intensity factor on the crack length. As expected, the presence of applied electric displacement loads will enhance the singular electric displacement ahead of an impermeable crack tip. Note that even in the case of absent applied electric displacement load the electric displacement intensity factor is not zero, which means that the applied mechanical stress can produce electric displacement intensity factors ahead of the crack tip. This property is quite different from the result for a crack in an infinite piezoelectric medium. In that case it is well known that the stress and electric displacement intensity are uncoupled, i.e., only electric displacement load can produces the singularity electric displacement ahead of the crack tip. The results in Fig. 7 also suggest that for a permeable or so-called electrically conducting crack, at a given crack length the electric displacement factor depends on the applied mechanical stress but not on the applied electric displacement load. Consequently, there is

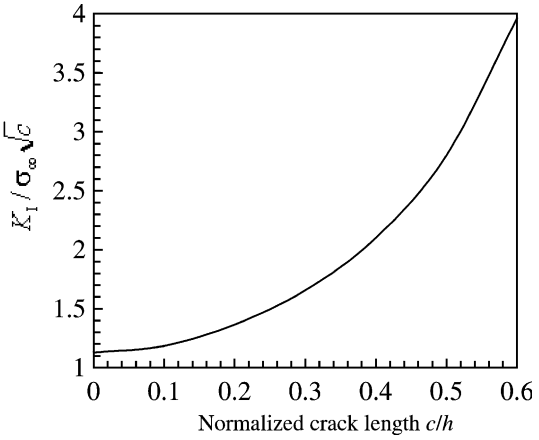

Fig. 6. Stress intensity factors versus crack length for an edge-cracked strip under the combination of a uniform tension load σ_∞ and a uniform electric displacement load D_∞ at the far ends. The applied electrical load and crack face electrical boundary condition assumptions have no influence on the stress intensity factor.

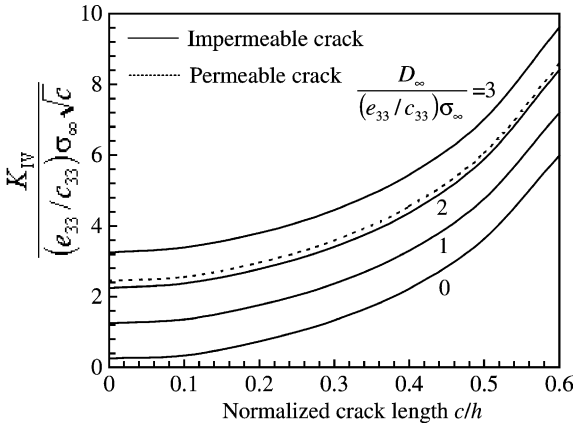

Fig. 7. Electric displacement intensity factors versus crack length for an edge-cracked strip under the combination of a uniform tension load σ_∞ and a uniform electric displacement load D_∞ at the far ends.

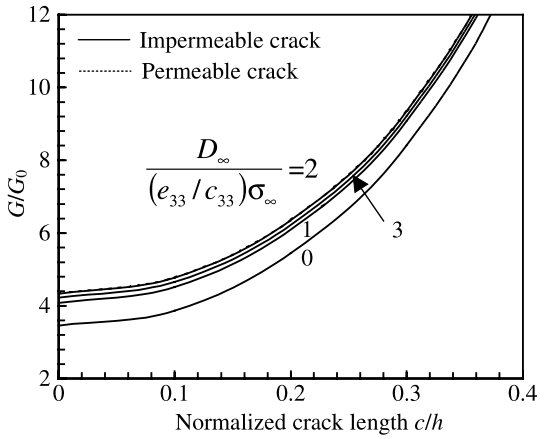

Fig. 8. Energy release rates versus crack length for an edge-cracked strip under the combination of a uniform tension load σ_∞ and a uniform electric displacement load D_∞ at the far ends, $G_0 = (\pi/2)\sigma_\infty^2 a/c_{11}$.

only one curve in Fig. 7 for a permeable crack. This result confirms the conclusion obtained earlier for a crack perpendicular to the poling direction (Fulton and Gao, 2001; Wang et al., 2000a,b).

Fig. 8 displays the energy release rates for different applied electric loads. It can be shown that the permeable crack assumption always give a maximum energy release rate for a certain crack length. Again the energy release rates for the permeable crack do not depend on the applied electric displacement load.

The deformed edge crack shapes are shown in Fig. 9 for different applied electric loads. It is found that in the regions of applied loads considered, the presence of electrical loads tends to make the impermeable crack more open. The shape of a permeable crack is dependent only on the applied mechanical stresses.

As mentioned above, the permeable crack model assumes that the crack is electrically conductive and the electric potential difference across the crack faces is zero. On the other hand, the impermeable crack model assumes that the crack is electrically insulated and the electric field inside the crack is zero but there is an electric potential difference across the crack for a certain applied load and they are plotted in Fig. 10. The

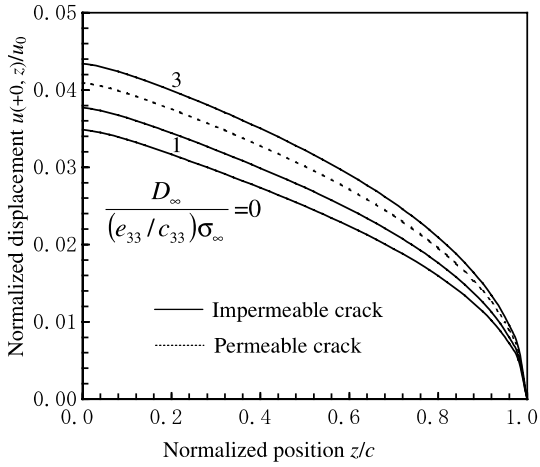

Fig. 9. The shape of the deformed edge crack. The strip undergoes a uniform tension load σ_∞ and a uniform electric displacement load D_∞ at the far ends, $u_0 = c\sigma_\infty/c_{33}$, $c = 0.2h$.

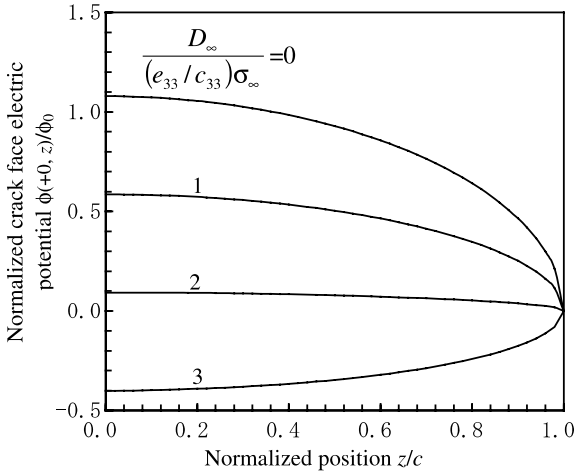

Fig. 10. The electric potential on the surface of an impermeable crack. The edge-cracked strip undergoes a uniform tension load σ_∞ and a uniform electric displacement load D_∞ at the far ends, $\phi_0 = c\sigma_\infty e_{33}/c_{33}\epsilon_{33}$, $c = 0.2h$.

figure shows that the electric potential on the crack face can be negative or positive depend on the applied electric displacement load.

Figs. 11–15 plot the stress intensity factors, electric displacements intensity factors, the energy release rates, the deformed crack shapes and the electric potentials on the crack face, respectively, for the edge-cracked strip under a pure bending moment and a uniform electric displacement at the far ends. The results for the double edge-cracked (DEC) strip under a uniform tension and a uniform electric displacement at the far ends are displayed in Figs. 16–20. Plotted in Figs. 21–25 are the results for the center-cracked strip under a uniform tension and a uniform electric displacement at the far ends. The effects of electrical boundary condition assumptions and the crack length for those crack and load configurations are similar to those for a single edge-cracked (SEC) strip under a uniform stress and electric displacement at the far ends.

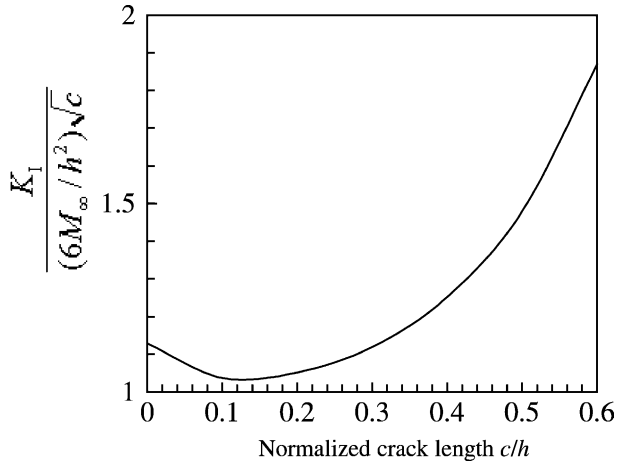

Fig. 11. Stress intensity factors versus crack length for an edge-cracked strip under the combination of a pure bending moment M_∞ and a uniform electric displacement load D_∞ at the far ends. The applied electrical load and crack face electrical boundary condition assumptions have no influence on the stress intensity factor.

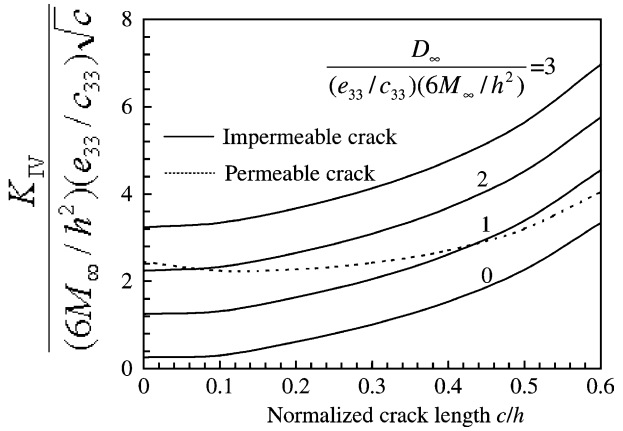

Fig. 12. Electric displacement intensity factors versus crack length for an edge-cracked strip under the combination of a pure bending moment M_∞ and a uniform electric displacement load D_∞ at the far ends.

6. Conclusions

A piezoelectric material strip with a crack normal to its surfaces is considered. The poling axis is assumed to be orthogonal to the crack plane. The remote mechanical stresses and electric displacements act at the infinite distance. The standard methods of Fourier transforms and singular integral equations are utilized. Both permeable and impermeable (insulated) crack face electrical boundary conditions are considered. Investigated specimens include an edge-cracked strip under uniform tension or pure bending, a DEC strip under uniform tension, and a center-cracked strip under tension.

For an impermeable crack problem, it is found that the electric displacement intensity factor depends both on the applied mechanical load and applied electric displacement load. For a permeable crack, the

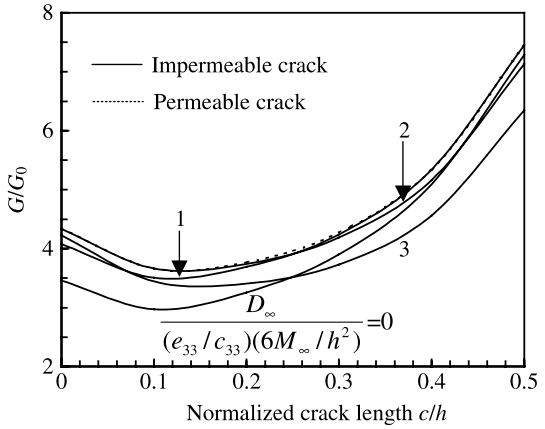

Fig. 13. Energy release rates versus crack length for an edge-cracked strip under the combination of a pure bending moment M_∞ and a uniform electric displacement load D_∞ at the far ends, $G_0 = (\pi/2)(6M_\infty/h^2)^2 a/c_{11}$.

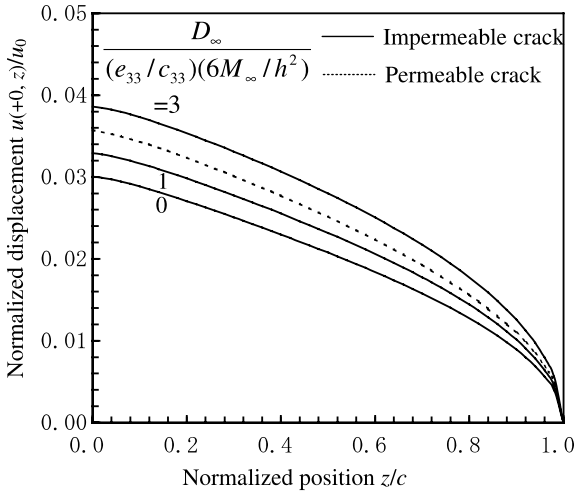

Fig. 14. The shape of the deformed edge crack, the strip undergoes a pure bending moment M_∞ and a uniform electric displacement load D_∞ at the far ends, $u_0 = c(6M_\infty/h^2)/c_{33}$, $c = 0.2h$.

electric displacement intensity factor depends on the applied mechanical load but not on the applied electric displacement load.

It is worthwhile to comment the results obtained from electrically permeable crack assumption. As mentioned above, according to the permeable crack assumption, the electric loads would have no influence on the singular stress and electric displacement ahead of the crack tip. Consequently, if permeable crack model is used to analyze the crack instability, the applied electric displacement load should contribute nothing to the fracture load. Such a conclusion would contradict experimental findings for it finds that the presence of an electric load can either promote or retard crack growth, depending on the magnitude and the direction of the electric load (Park and Sun, 1995a,b; Pak and Tobin, 1993). Hence, the permeable assumption is not able to predict the fracture strength of piezoelectric materials correctly, and this assumption may not directly be applied to the fracture problems of piezoelectric materials unless other approaches are

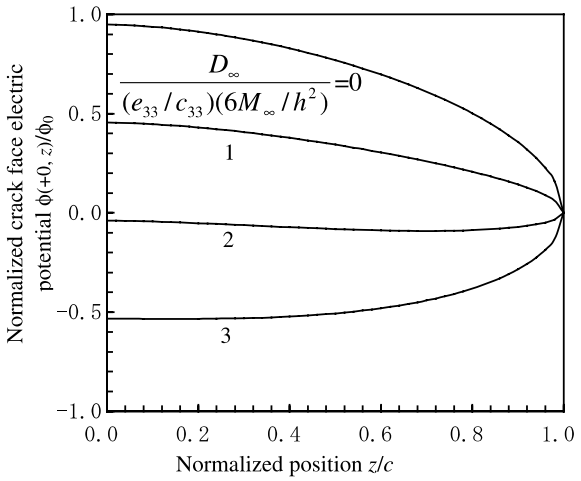

Fig. 15. The electric potential on the surface of an impermeable crack. The edge-cracked strip undergoes a pure bending moment M_∞ and a uniform electric displacement load D_∞ at the far ends, $\phi_0 = c(6M_\infty/h^2)e_{33}/c_{33}\epsilon_{33}$, $c = 0.2h$.

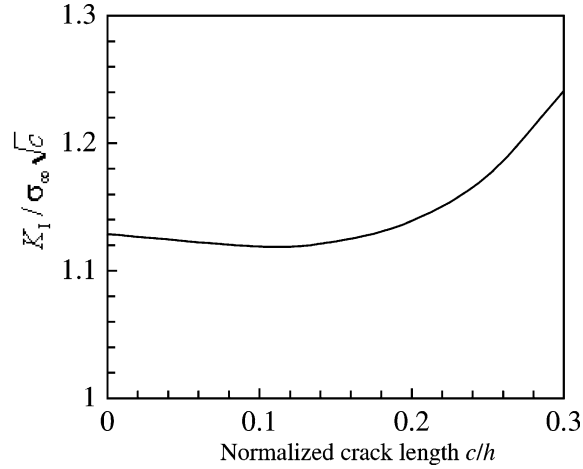

Fig. 16. Stress intensity factors versus crack length for a DEC strip under the combination of a uniform tension load σ_∞ and a uniform electric displacement load D_∞ at the far ends. The applied electrical load and crack face electrical boundary condition assumptions have no influence on the stress intensity factor.

involved. An approach which seems to be somewhat consistent and overcomes the difficult of the permeable crack assumption is to take the deformation of the crack into account (McMeeking, 1999). This approach has been used before in analytical solutions and in finite element treatments (McMeeking, 1999, 2001; Xu and Rajapakse, 2001; Zhang et al., 1998).

Appendix A

$$C_{1m} = c_{44}\lambda_m A_{1m} - c_{44}A_{2m} + e_{15}\lambda_m A_{3m}$$

$$D_{1n} = -\mathrm{i}c_{44}B_{1n} + c_{44}\,\mathrm{sgn}(\xi)\lambda_n B_{2n} - \mathrm{i}e_{15}B_{3n}$$

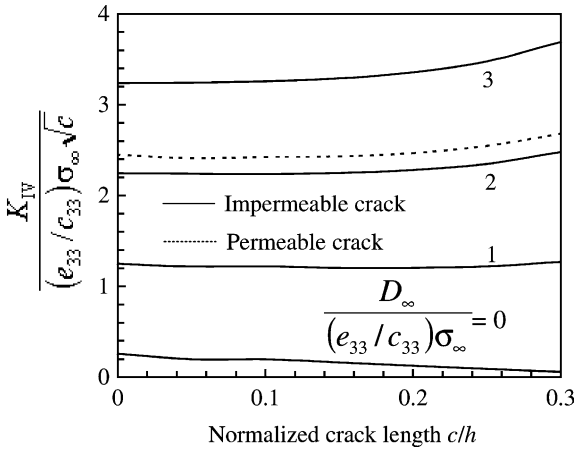

Fig. 17. Electric displacement intensity factors versus crack length for a DEC strip under the combination of a uniform tension load σ_∞ and a uniform electric displacement load D_∞ at the far ends.

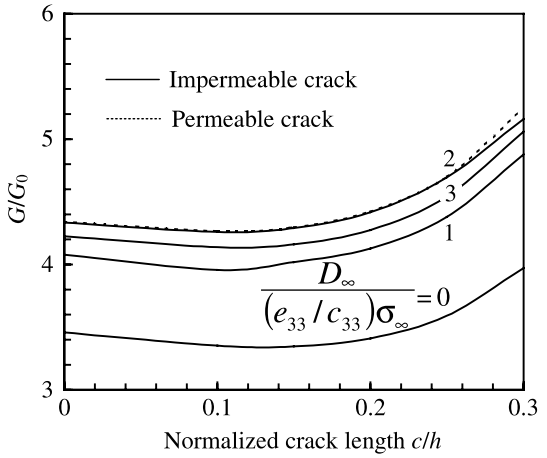

Fig. 18. Energy release rates versus crack length for a DEC strip under the combination of a uniform tension load σ_∞ and a uniform electric displacement load D_∞ at the far ends, $G_0 = (\pi/2)\sigma_\infty^2 a/c_{11}$.

$$C_{2m} = c_{13}A_{1m} + c_{11}\lambda_m A_{2m} + e_{31}A_{3m}$$

$$D_{2n} = c_{13}\,\mathrm{sgn}(\xi)\lambda_n B_{1n} - \mathrm{i}c_{11}B_{2n} + e_{31}\,\mathrm{sgn}(\xi)\lambda_n B_{3n}$$

$$C_{3m} = e_{15}\lambda_m A_{1m} - e_{15}A_{2m} - \epsilon_{11}\lambda_m A_{3m}$$

$$D_{3n} = -\mathrm{i}e_{15}B_{1n} + e_{15}\,\mathrm{sgn}(\xi)\lambda_n B_{2n} + \mathrm{i}\epsilon_{11}B_{3n}$$

$$C_{4m} = c_{33}A_{1m} + c_{13}\lambda_m A_{2m} + e_{33}A_{3m}$$

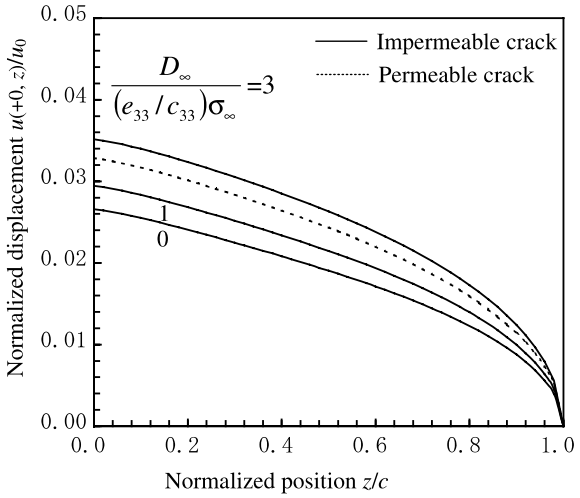

Fig. 19. The shape of the deformed double edge crack. The strip undergoes a uniform tension load σ_∞ and a uniform electric displacement load D_∞ at the far ends, $u_0 = c\sigma_\infty/c_{33}$, $c = 0.2h$.

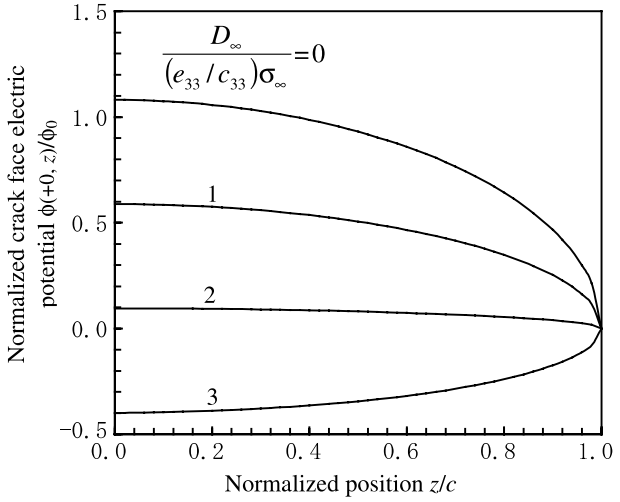

Fig. 20. The electric potential on the surface of an impermeable crack. The DEC strip undergoes a uniform tension load σ_∞ and a uniform electric displacement load D_∞ at the far ends, $\phi_0 c\sigma_\infty e_{33}/c_{33}\epsilon_{33}$, $c = 0.2h$.

$$D_{4n} = c_{33}\,\mathrm{sgn}(\xi)\lambda_n B_{1n} - \mathrm{i}c_{13}B_{2n} + e_{33}\,\mathrm{sgn}(\xi)\lambda_n B_{3n}$$

$$C_{5m} = e_{33}A_{1m} + e_{31}\lambda_m A_{2m} - \epsilon_{33}A_{3m}$$

$$D_{5n} = e_{33}\,\mathrm{sgn}(\xi)\lambda_n B_{1n} - \mathrm{i}e_{31}B_{2n} - \epsilon_{33}\,\mathrm{sgn}(\xi)\lambda_n B_{3n}$$

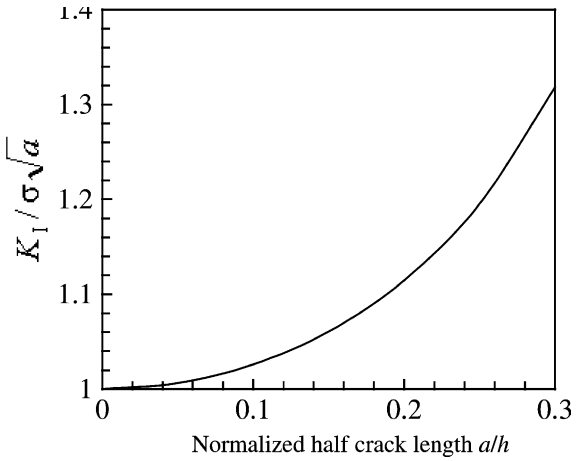

Fig. 21. Stress intensity factors versus crack length for a center-cracked strip under the combination of a uniform tension load $_\infty$ and a uniform electric displacement load D_∞ at the far ends. The applied electrical load and crack face electrical boundary condition assumptions have no influence on the stress intensity factor.

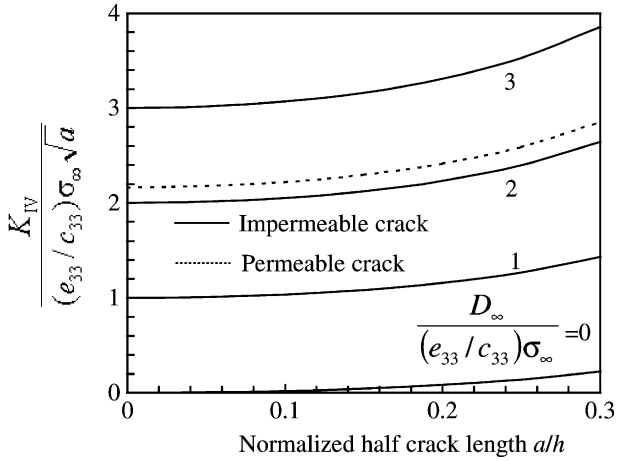

Fig. 22. Electric displacement intensity factor versus crack length for a center-cracked strip under the combination of a uniform tension load σ_∞ and a uniform electric displacement load D_∞ at the far ends.

Appendix B

$$b_{1u} = (B_{32}D_{13} - B_{33}D_{12})/\Delta, \quad b_{1\phi} = (B_{13}D_{12} - B_{12}D_{13})/\Delta,$$

$$b_{2u} = (B_{33}D_{11} - B_{31}D_{13})/\Delta, \quad b_{2\phi} = (B_{11}D_{13} - B_{13}D_{11})/\Delta,$$

$$b_{3u} = (B_{31}D_{12} - B_{32}D_{11})/\Delta, \quad b_{3\phi} = (B_{12}D_{11} - B_{11}D_{12})/\Delta,$$

$$\Delta = B_{11}(B_{32}D_{13} - B_{33}D_{12}) + B_{12}(B_{33}D_{11} - B_{31}D_{13}) + B_{13}(B_{31}D_{12} - B_{32}D_{11}).$$

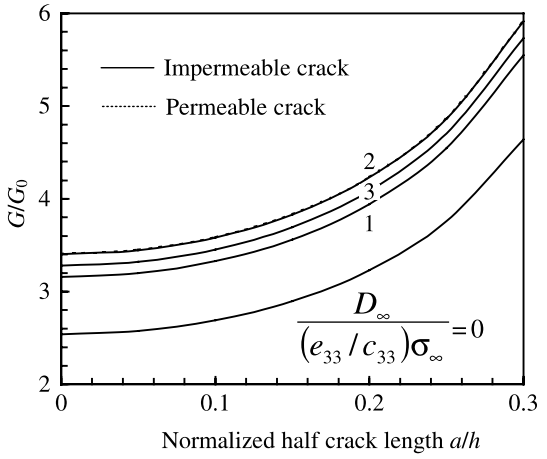

Fig. 23. Energy release rate versus crack length for a center-cracked strip under the combination of a uniform tension load σ_∞ and a uniform electric displacement load D_∞ at the far ends, $G_0 = (\pi/2)\sigma_\infty^2 a/c_{11}$.

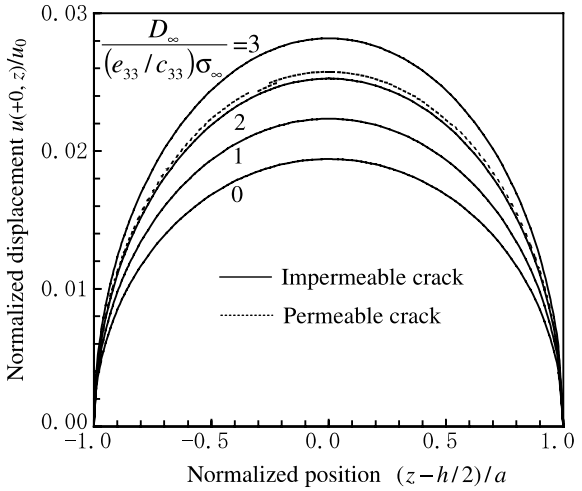

Fig. 24. The shape of the deformed center crack. The center-cracked strip undergoes the combination of a uniform tension load α_∞ and a uniform electric displacement load D_∞ at the far ends, $u_0 = a\sigma_\infty/c_{33}$, $a = 0.2h$.

Appendix C

If stress free boundary condition (9a) is used, then

$$[G] = \begin{bmatrix} C_{11}e^{s\lambda_1 h} & C_{12}e^{s\lambda_2 h} & C_{13}e^{s\lambda_3 h} & C_{14}e^{s\lambda_4 h} & C_{15}e^{s\lambda_5 h} & C_{16}e^{s\lambda_6 h} \\ C_{11} & C_{12} & C_{13} & C_{14} & C_{15} & C_{16} \\ C_{21}e^{s\lambda_1 h} & C_{22}e^{s\lambda_2 h} & C_{23}e^{s\lambda_3 h} & C_{24}e^{s\lambda_4 h} & C_{25}e^{s\lambda_5 h} & C_{26}e^{s\lambda_6 h} \\ C_{21} & C_{22} & C_{23} & C_{24} & C_{25} & C_{26} \\ C_{31}e^{s\lambda_1 h} & C_{32}e^{s\lambda_2 h} & C_{33}e^{s\lambda_3 h} & C_{34}e^{s\lambda_4 h} & C_{35}e^{s\lambda_5 h} & C_{36}e^{s\lambda_6 h} \\ C_{31} & C_{32} & C_{33} & C_{34} & C_{35} & C_{36} \end{bmatrix},$$

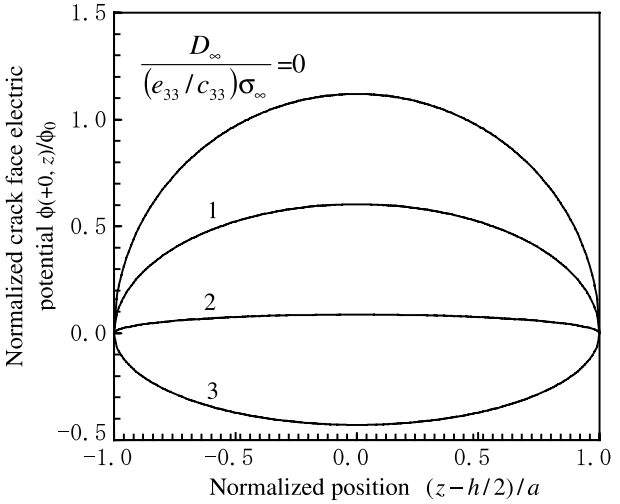

Fig. 25. The electric potential on the surface of an impermeable crack. The center-cracked strip undergoes the combination of a uniform tension load σ_∞ and a uniform electric displacement load D_∞ at the far ends, $\phi_0 = a\sigma_\infty e_{33}/c_{33}\epsilon_{33}$, $a = 0.2h$.

and the vectors $\{f_u\}$ and $\{f_\phi\}$ are:

$$\{f_u\} = (f_{1u} \quad f_{2u} \quad f_{3u} \quad f_{4u} \quad f_{5u} \quad f_{6u})^{\mathrm{T}}$$

$$\{f_\phi\} = (f_{1\phi} \quad f_{2\phi} \quad f_{3\phi} \quad f_{4\phi} \quad f_{5\phi} \quad f_{6\phi})^{\mathrm{T}}.$$

If bending free boundary condition (9b) is considered, then C_{2m} in the third row of matrix $[G]$ should be replaced by A_{2m} $(m = 1, \ldots, 6)$, and the vectors $\{f_u\}$ and $\{f_\phi\}$ should be

$$\{f_u\} = (f_{1u} \quad f_{2u} \quad f_{7u} \quad f_{4u} \quad f_{5u} \quad f_{6u})^{\mathrm{T}}$$

$$\{f_\phi\} = (f_{1\phi} \quad f_{2\phi} \quad f_{7\phi} \quad f_{4\phi} \quad f_{5\phi} \quad f_{6\phi})^{\mathrm{T}}.$$

In above expressions, the elements in vectors $\{f_u\}$ and $\{f_\phi\}$ are:

$$f_{1u}(s,r) = -\frac{\mathrm{i}}{\pi}\sum_{n=1}^{3}\int_{-\infty}^{\infty}\frac{s}{\xi^2\lambda_n^2+s^2}D_{1n}b_{nu}\mathrm{e}^{\mathrm{i}\xi(r-h)}\,\mathrm{d}\xi = -\sum_{n=1}^{3}\mathrm{Im}(D_{1n}b_{nu}\mathrm{e}^{s(h-r)/\lambda_n}/\lambda_n),$$

$$f_{2u}(s,r) = -\frac{\mathrm{i}}{\pi}\sum_{n=1}^{3}\int_{-\infty}^{\infty}\frac{s}{\xi^2\lambda_n^2+s^2}D_{1n}b_{nu}\mathrm{e}^{\mathrm{i}\xi r}\,\mathrm{d}\xi = -\sum_{n=1}^{3}\mathrm{Im}(D_{1n}b_{nu}\mathrm{e}^{sr/\lambda_n}/\lambda_n),$$

$$f_{3u}(s,r) = \frac{\mathrm{i}}{\pi}\sum_{n=1}^{3}\int_{-\infty}^{\infty}\frac{|\xi|\lambda_n}{\xi^2\lambda_n^2+s^2}D_{2n}b_{nu}\mathrm{e}^{\mathrm{i}\xi(r-h)}\,\mathrm{d}\xi = \sum_{n=1}^{3}\mathrm{Re}(D_{2n}b_{nu}\mathrm{e}^{s(h-r)/\lambda_n}/\lambda_n),$$

$$f_{4u}(s,r) = \frac{\mathrm{i}}{\pi}\sum_{n=1}^{3}\int_{-\infty}^{\infty}\frac{|\xi|\lambda_n}{\xi^2\lambda_n^2+s^2}D_{2n}b_{nu}\mathrm{e}^{\mathrm{i}\xi r}\,\mathrm{d}\xi = -\sum_{n=1}^{3}\mathrm{Re}(D_{2n}b_{nu}\mathrm{e}^{sr/\lambda_n}/\lambda_n),$$

$$f_{5u}(s,r) = -\frac{\mathrm{i}}{\pi}\sum_{n=1}^{3}\int_{-\infty}^{\infty}\frac{s}{\xi^2\lambda_n^2+s^2}D_{3n}b_{nu}\mathrm{e}^{\mathrm{i}\xi(r-h)}\,\mathrm{d}\xi = -\sum_{n=1}^{3}\mathrm{Im}(D_{3n}b_{nu}\mathrm{e}^{s(h-r)/\lambda_n}/\lambda_n),$$

$$f_{6u}(s,r) = -\frac{\mathrm{i}}{\pi}\sum_{n=1}^{3}\int_{-\infty}^{\infty}\frac{s}{\xi^2\lambda_n^2+s^2}D_{3n}b_{nu}\mathrm{e}^{\mathrm{i}\xi r}\,\mathrm{d}\xi = -\sum_{n=1}^{3}\mathrm{Im}(D_{3n}b_{nu}\mathrm{e}^{sr/\lambda_n}/\lambda_n),$$

$$f_{7u}(s,r) = \frac{\mathrm{i}}{\pi}\sum_{n=1}^{3}\int_{-\infty}^{\infty}\frac{s\,\mathrm{sgn}(\xi)\lambda_n}{\xi^2\lambda_n^2+s^2}B_{2n}b_{nu}\mathrm{e}^{\mathrm{i}\xi(r-h)}\,\mathrm{d}\xi = \sum_{n=1}^{3}\mathrm{Im}(B_{2n}b_{nu}\mathrm{e}^{s(h-r)/\lambda_n}).$$

$f_{i\phi}$ can be obtained by replacing the subscript u in the above expressions with ϕ. Obviously, f_{iu} and $f_{i\phi}$ $(i = 1,\ldots,7)$ are pure real numbers. When evaluating the above infinity integrals, we have used the theory of residues. Further, D_{jn} and b_{nu} $(j,n = 1,2,3)$ at the right hand side of f_{ju} $(j = 1, j = 7)$ are evaluated for $\mathrm{sgn}(kc) = 1$.

References

Balke, H., Kemmer, G., Drescher, J., 1997. Some remarks on fracture mechanics of piezoelectric solids. In: Michel, B., Winkler, T. (Eds.), Proceeding of the Micro Materials Conference MicroMat'97, Berlin, pp. 398–401.

Beom, H.G., Atluri, S.N., 1996. Near-tip fields and intensity factors for interfacial cracks in dissimilar anisotropic piezoelectric media. International Journal of Fracture 75, 163–183.

Dunn, M.L., 1994. The effects of crack face boundary conditions on the fracture of piezoelectric solids. Engineering Fracture Mechanics 48, 25–39.

Erdogan, F., Wu, B.H., 1996. Crack problem in FGM layers under thermal stresses. Journal of thermal stresses 19, 237–265.

Erdogan, F., Wu, B.H., 1997. The surface crack problem for a plate with functionally graded properties. ASME Journal of Applied Mechanics 64, 449–456.

Fulton, C.C., Gao, H., 2001. Effect of local polarization switching on piezoelectric fracture. Journal of Mechanics and Physics of Solids 49, 927–952.

Hao, T.-H., Shen, Z.-Y., 1994. A new electric boundary condition of electric fracture mechanics and its applications. Engineering Fracture Mechanics 47, 793–802.

Herrmann, K.P., Loboda, V.V., Govorukha, V.B., 2001. On contact zone models for an electrically impermeable interface crack in a piezoelectric bimaterial. International Journal of Fracture 111, 203–227.

Kwon, S.M., Lee, K.Y., 2000. Analysis of stress and electric fields in a rectangular piezoelectric body with a center crack under anti-plane shear loading. International Journal of Solids and Structures 37, 4859–4869.

McMeeking, R.M., 1999. Crack tip energy release rate for a piezoelectric compact tension specimen. Engineering Fracture Mechanics 64, 217–244.

McMeeking, R.M., 2001. Towards a fracture mechanics for brittle piezoelectric and dielectric materials. International Journal of Fracture 108, 25–41.

Mikahailov, G.K., Parton, V.Z., 1990. Electromagnetoelasticity. Hemisphere, New York.

Pak, Y.E., 1990. Crack extension force in a piezoelectric material. Journal of Applied Mechanics 57, 647–653.

Pak, Y.E., Tobin, A., 1993. On electric field effects in fracture of piezoelectric material. In: Lee, J.S., Maugin, G.A., Shindo, Y. (Eds.), ASME Mechanics of Electromagnetic Materials and Structures, AMD-vol. 161, MD-vol. 42, pp. 51–62.

Park, S.B., Sun, C.T., 1995a. Effect of electric field on fracture of piezoelectric ceramics. International Journal of Fracture 70, 203–216.

Park, S., Sun, C.T., 1995b. Fracture criteria for piezoelectric ceramics. Journal of American Ceramic Society 78, 1475–1480.

Qin, Q.H., Mai, Y.W., 1999. A closed crack model for interface cracks in thermopiezoelectric materials. International Journal of Solids and Structures 36, 2463–2479.

Shindo, Y., Watanabe, K., Narita, F., 2000. Electroelastic analysis of a piezoelectric ceramic strip with a central crack. International Journal of Engineering Science 38, 1–19.

Sih, G.C., Zuo, J.Z., 2000. Multiscale behavior of crack initiation and growth in piezoelectric ceramics. Theoretical and Applied Fracture Mechanics 34, 123–141.

Soh, A.K., Fang, D.N., Lee, K.L., 2001. Fracture analysis of piezoelectric materials with defects using energy density theory. International Journal of Solids and Structures 38, 8331–8344.

Sosa, H., 1991. Plane problems in piezoelectric media with defects. International Journal of Solids and Structures 28, 491–506.

Suo, Z., Kuo, C.M., Barnett, D.M., Willis, J.R., 1992. Fracture mechanics for piezoelectric ceramics. Journal of Mechanics and Physics of Solids 40, 739–765.

Wang, T.C., 2000. Analysis of strip electric saturation model of crack problem in piezoelectric materials. International Journal of Solids and Structures 37, 6031–6049.

Wang, B.L., Noda, N., 2000. Mixed mode crack initiation in piezoelectric Ceramic Strip. Theoretical and Applied Fracture Mechanics 34, 35–47.

Wang, B.L., Noda, N., 2001a. Thermal induced fracture of a smart functionally graded composite structure. Theoretical and Applied Fracture Mechanics 35, 93–109.

Wang, B.L., Noda, N., 2001b. Axisymmetric deformation for of piezoelectric multilayers. Philosophical Magazine Part A 81, 1009–1019.

Wang, B.L., Han, J.C., Du, S.Y., 1998. Dynamic response for non-homogeneous piezoelectric medium with multiple cracks. Engineering Fracture Mechanics 61, 607–617.

Wang, B.L., Han, J.C., Du, S.Y., 2000a. New considerations for the fracture of piezoelectric materials under electromechanical loading. Mechanics Research Communications 27, 435–444.

Wang, B.L., Han, J.C., Du, S.Y., 2000b. Electroelastic fracture dynamics for multilayered piezoelectric materials under dynamic anti-plane shearing. International Journal of Solids and Structures 37, 5219–5231.

Xu, X.L., Rajapakse, R.K.N.D., 2001. On a plane crack in piezoelectric solids. International Journal of Solids and Structures 38, 7643–7658.

Zhang, T.Y., Tong, P., 1996. Fracture Mechanics for a mode-III crack in a piezoelectric material. International Journal of Solids and Structures 33, 343–359.

Zhang, T.Y., Qian, C.F., Tong, P., 1998. Linear electro-elastic analysis of a cavity or a crack in a piezoelectric material. International Journal of Solids and Structures 35, 2121–2149.